Journal of Coastal Research	SI 39	1570 - 1573	ICS 2004 (Proceedings)	Brazil	ISSN 0749-0208

Wave Induced Flow and Hydraulic Performances of Porous Seawall

M. F. Karim and K. Tanimoto

Department of Civil and
Environmental Engineering
Saitama University, Saitama
338-8570, Japan
sgd3051@post.saitama-u.ac.jp

ABSTRACT

KARIM, M.F. and TANIMOTO, K., 2006. Wave induced flow and hydraulic performances of porous seawall. Journal of Coastal Research, SI 39 (Proceedings of the 8th International Coastal Symposium), 1570 - 1573. Itajaí, SC, Brazil, ISSN 0749-0208.

The knowledge of wave motion in and around the artificial porous structures, such as breakwaters and seawalls is the key issue to determine the functionality and stability of those structures. A study is conducted to investigate the nonlinear interactions between wave-induced flow and porous structures, and to assess the hydraulic performances of porous seawalls. The study is done by developing a numerical model based on adapted Navier-Stokes equations for porous medium. A two-phase flow model is incorporated with the porous flow model considering finite thickness of air zone above the wave domain. The advection of free surface is modeled by the volume of fluid method. The resistance to wave propagation due to porous medium is modeled in terms of inertia and drag forces. The model is calibrated and verified with experimental results. It is then applied to investigate the influences of wave and structural parameters on the hydraulic performances. The results showed that there exists optimum structure width for which wave reflection is the minimum. The positive role of porosity in reducing wave reflection is confirmed. The wave height at the rear wall decreases exponentially with increasing structure width and increases with porosity increasing. Finally, velocity distributions in and around the structure are investigated. The velocity decreases through the structure significantly and near the rear wall it approaches zero. The findings of this research provide a background and give some valuable information to the researchers and designers working in the field of coastal engineering.

ADDITIONAL INDEX WORDS: *Two-phase model, VOF method, reflection.*

INTRODUCTION

Artificial porous structures such as rubble mound breakwaters, seawalls, submerged structures, outfall protections, artificial reefs or armor layers for the protection of seawalls or vertical structures are of great interest in coastal and harbor engineering, since they provide one of the best means to induce incident wave dissipation by friction inside the structure. These structures are designed mainly to provide protection by reflection and/or dissipation of wave energy. For maximizing the hydraulic performances of such structures, it is essential to maximize dissipation and minimize reflection. In general, a wave train through porous structure is reflected, transmitted and dissipated. All these processes induce significant changes in the wave properties inside the porous structure. The degree of influence, however, depends on the structural parameters and incident wave conditions. Therefore, it is essential to investigate the influences of all these parameters on functional variables such as reflection and wave height at the rear wall. Due to the complexities of both porous flow and nonlinear wave behavior, the problems related to it are extremely difficult to solve and are being investigated for many years. However, the mechanism of wave energy dissipation and reflection due to porous structure is not understood clearly yet.

The wave transformation in porous structure has been investigated by experimental studies and analytical models (MALLAYACHARI and SUNDAR, 1994; van GENT, 1995). Hydraulic experiments, however, contain the scale effects. On the other hand, analytical solutions are based on a set of assumptions which limits the applicability of the models. Therefore, numerical models are the essential tools for the investigation of nonlinear wave transformation in porous structure. SAKAKIYAMA and KAJIMA (1992), and van GENT (1995) proposed numerical models based on the direct numerical simulation of adapted Navier-Stokes equations for porous medium. All these studies are the one-phase models, in which the effect of air movement above the free surface is ignored. As a result, water splash in the air or entrapped air in the water is not fully treated. In addition to this problem, one-phase model requires extrapolation or interpolation for physical variables (pressure and velocity) at the interface boundary between air and water. Occasionally, this approximation leads to the source of error in the solution domain. One of the methods to improve is to introduce the two-phase model of water and air considering finite air zone above the free surface (SUSSMAN *et al*., 1994; HIEU and TANIMOTO, 2002). The wave motion in porous media, however, was not considered in those studies. Based on HIEU and TANIMOTO (2002) model, KARIM *et al.* (2003) developed a volume of fluid (VOF) based two-phase model to simulate wave transformation in porous structure. In the present study, level set function proposed by SUSSMAN *et al*. (1994) is introduced in KARIM *et al.* (2003) model to improve the numerical stability.

METHOD OF SIMULATIONS

Model Equations

In the present research, porous flow model is based on the adapted Navier-Stokes equations and continuity equation (SAKAKIYAMA and KAJIMA, 1992);

$$\frac{\partial(\gamma_j u_j)}{\partial x_j} = 0 \tag{1}$$

$$\lambda_v \frac{\partial u_i}{\partial t} + \frac{\partial(\lambda_j u_j u_i)}{\partial x_j} = -\frac{\gamma_v}{\rho}\frac{\partial p}{\partial x_i} + \frac{\partial}{\partial x_j}[\gamma_j \nu_e (\frac{\partial u_i}{\partial x_j} + \frac{\partial u_j}{\partial x_i})] + \gamma_v g_i - R_i \tag{2}$$

$$R_i = \frac{1}{2}\frac{C_D}{\Delta x_i}(1-\gamma_i)\,u_i\sqrt{u_j^2} \qquad (3)$$

where i=1, 2 corresponds to coordinate axis and j=1, 2 is dummy suffix, x_i is the coordinate, u_i the velocity component, g_i the gravitational acceleration, ρ the density, p the pressure, υ_e the kinematic viscosity, γ_v the volume porosity, γ_i the surface permeability, $\lambda=\gamma+(1-\gamma)C_M$, R_i the drag force, C_M the inertia coefficient, C_D the drag coefficient.

The advection of free surface is treated by the volume of fluid (VOF) method (HIRT and NICHOLS, 1981) in terms of VOF function F and the advection equation of F function is solved by HARVIE and FLETCHER (2001) scheme. The physical meaning of F is the fractional volume of a cell occupied by fluid. It can vary between zero (empty cell) and one (full of fluid). The cells having F value between zero and one must then contain a free surface. The advection of F is governed by

$$\frac{\partial(\gamma_v F)}{\partial t} + \frac{\partial(\gamma_j u_j F)}{\partial x_j} = 0 \qquad (4)$$

The two-phase flow model is governed by the advection of density and viscosity. The fluids in two layers are assumed to be incompressible. For immiscible liquids the density and viscosity are constant on particle paths and these are expressed as:

$$\frac{\partial(\gamma_v \rho)}{\partial t} + \frac{\partial(\gamma_j u_j \rho)}{\partial x_j} = 0 \qquad (5)$$

$$\frac{\partial(\gamma_v \nu_e)}{\partial t} + \frac{\partial(\gamma_j u_j \nu_e)}{\partial x_j} = 0 \qquad (6)$$

Since, ρ and υ_e change sharply at the interface, conventional finite difference schemes will incur excessive numerical diffusion. To avoid this problem, the equations are solved in terms of F as follows:

$$\rho = (1-F)\rho_{air} + F\rho_{water} \qquad (7)$$

$$\nu_e = (1-F)(\nu_e)_{air} + F(\nu_e)_{water} \qquad (8)$$

The numerical instability may still occur when solving momentum equation (Equation 2) due to large density ratio of water and air. To avoid this problem, smoothing of density function is done at the interface as proposed by SUSSMAN *et al*. (1994).

Numerical Implementation

The governing equations are discretized using finite difference technique on a staggered grid system. In the computation, the velocity components u and w, and the pressure p at the next time step are calculated using the SMAC procedure (Equation 1 and 2). Then, using the calculated velocity, the new free surface configuration is computed with the advection equation of VOF function F (Equation 4). The density and viscosity are then updated (Equation 7 and 8).

In the present study, boundary conditions for resolved field are categorized into two kinds, namely, inflow boundary and the mesh boundary conditions. At the inflow boundary, a piston type wave maker with reflected wave absorbing mechanism is introduced to generate the incident wave. The wave paddle is driven by the second order Stokes wave theory. The mesh boundary of continuative condition is adopted at the top while free slip condition is adopted at the left, right and bottom boundaries. It is worthy mentioning that no boundary condition is needed at the surface boundary of porous structure because the continuity equation reserves the continuity of variables at local cells. However, all the porous parameters are averaged at the interface.

CONDITIONS OF SIMULATIONS

The length and height of the numerical wave channel are 14.4 and 0.80 m respectively. Still water level is 0.375 m and the top boundary is set 0.425 m above the still water level. The height of the structure is 0.50 m, which satisfies the non-overtopping condition. The simulation is made for several structure widths and porosities but same height. The origin of x-axis is considered at the front face of the porous structure and the positive direction is the propagating direction of incident wave. At the backside of the structure an impermeable wall is considered which is termed as rear wall. Simulation of wave propagation was carried out for three wave periods T=1.2, 1.6 and 2.0 s, and several incident wave height H_i ranging from 0.03 to 0.12 m. The influences of different structural parameters namely width and porosity on reflection and wave height at the rear wall are investigated for a typical wave condition T=1.6 s and H_i=0.076 m for which H_i/h=0.20, H_i/L=0.028 and h/L=0.136 where h is still water depth and L is wave length. The porosity of the structure γ=0.43 and the resistance coefficients C_D=3.5 and C_M=0.5 are used for all wave and structural conditions (KARIM *et al*., 2003). Computational grid size is 0.02m in the horizontal direction (x-axis) and 0.01 m in the vertical direction (z-axis). Time increment is set by satisfying CFL and viscous stability conditions. The computation starts from still water condition. The surface displacement η at t=0 is null for whole computational region as well as u=w=0. The pressure at t=0 is given by the hydrostatic pressure. Total computational time is set for approximately 16 wave cycles. In

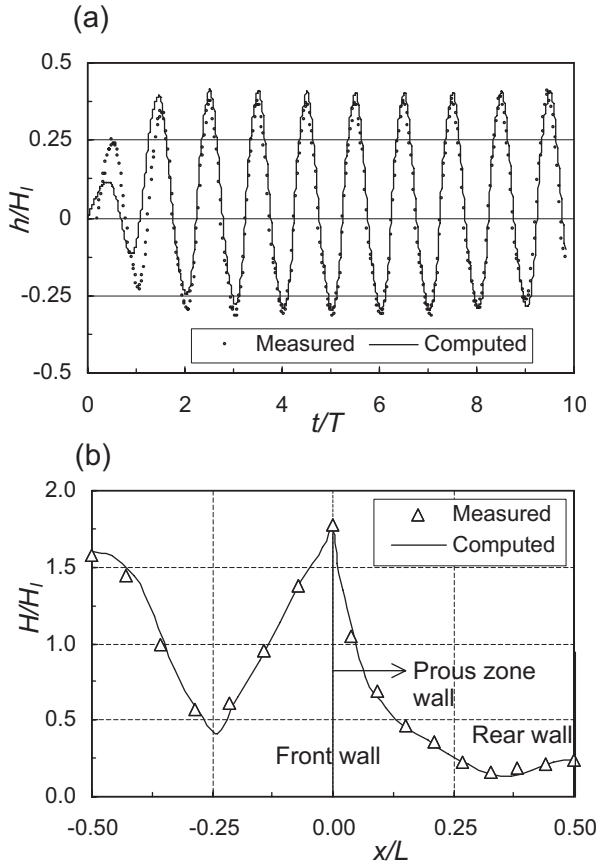

Figure 1. Comparison of a) time series of surface elevation inside the structure at 0.1L distance from the front wall b) wave height distributions inside and in front of the structure, for a typical wave conditions T=1.6 s, H_i=0.076 m, and structural conditions B/L=0.5, γ=0.43, D_m=0.025m.

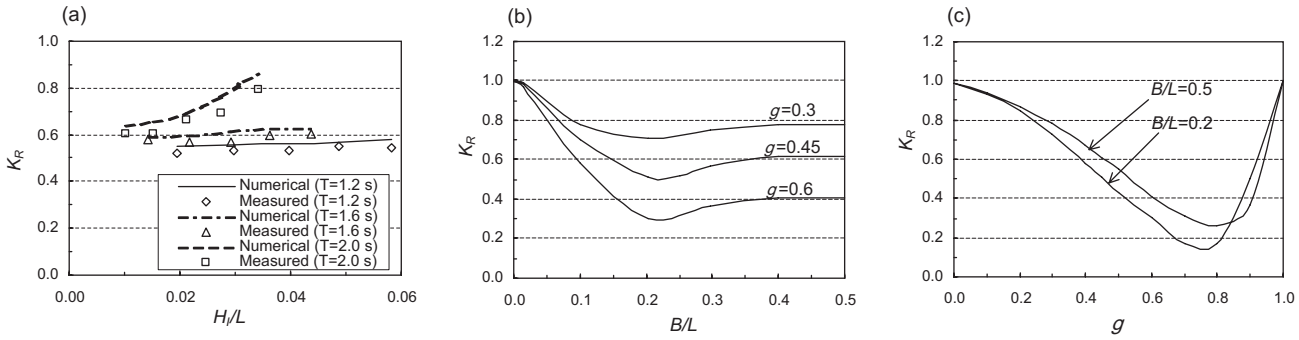

Figure 2. Reflection coefficients with (a) different incident wave conditions (b) structure width and (c) structure porosity. The results are shown for 3 wave periods and 5 wave heights in (a), while a typical wave condition T=1.6 s and H_I=0.076 m is considered in (b) and (c).

the analysis of numerical results, last 8 wave cycles are considered to avoid initial disturbances.

RESULTS AND DISCUSSIONS

Surface Elevation and Wave Height

A typical comparison of numerical results for water surface level and wave height distributions is shown in Figure 1. The upper figure (Figure 1a) shows the time series of surface elevations for a typical section inside porous structure (0.1L distance from front wall). It can be seen that numerical results agree well with measured data both in magnitude and phase excepting the transient state. The lower figure (Figure 1b) shows the comparison of wave height distributions both inside and in front of the structure. The front wall of the structure is at x/L=0 while the rear wall at x/L=0.5. A fairly good agreement is obtained between numerical and measured results both inside and outside the structure. At the front wall sharp change in the water surface elevation is occurred. This is due to sudden resistive force caused by porous medium and the reduction of flow area. Near the rear wall locally increased wave heights are observed. This is due to formation of partial standing wave in front of the rear wall. The incident wave is reflected partly by the front wall and partly by the rear wall. Due to the reflection, partial standing waves are formed both in front of the structure and in front of the rear wall. In general, wave height decreases exponentially inside the structure other than the rear wall.

Wave Reflection

The reflection coefficient K_R is defined as the ratio of reflected wave height H_R from the porous structure to the incident wave height H_I. The performance of the present numerical model was checked comparing computed reflection coefficients for different wave conditions with the experimental results. Figure 2a shows the K_R for a typical structural conditions B=1.38 m, D_m=0.025m, =0.43, and 15 wave conditions. The computed K_R for T=1.2 s and T=1.6 s are very close to experimental results while for T=2.0 s, there exist differences. However, the trend is same in all the cases. In general, numerical model predicts higher K_R but the difference is not large.

The influence of structure width on wave reflection is investigated in the range of B/L0.5 for T=1.6 s and H_I=0.076 m (Figure 2b). It can be seen that, for smaller relative widths, reflection coefficient decreases with increasing B/L and becomes the minimum for approximately B/L=0.2. Then, the reflection coefficient increases slightly for some extent and becomes almost constant in the range of B/L0.4. This is explained by the fact that outside the structure, influences of reflection from the rear wall becomes small, as the relative structure width increasing. The minimum condition is caused as the result of interaction between waves reflected at the front wall and at the rear wall with different phases. The results are shown for 3 representative porosities of 0.3, 0.45 and 0.6. The reflection is smaller for higher porosity for any relative width.

The variations of K_R with porosity for fixed values of other parameters are shown in Figure 2c. The results of two relative structure widths B/L=0.2 and B/L=0.5 are considered to assess the optimum structural condition. It shows that wave reflection is significantly influenced by porosity. For very small porosities, the structure behaves as if it had an impermeable front wall and the reflection coefficient tends to be 1.0 (no dissipation). For another extreme condition toward no porous materials with very high porosity, the behavior is similar but with the reflecting point at the rear wall. In between, there is a point of optimal porosity for which reflection coefficient is the minimum and energy dissipation is the maximum.

Wave Height at the Rear Wall

The numerical and experimental results for relative wave heights at the rear wall H_w/H_I with different incident wave conditions are shown in Figure 3a, where H_w is wave height at the rear wall. It shows that H_w/H_I decreases with wave steepness exponentially. The variations of H_w/H_I with structure width are

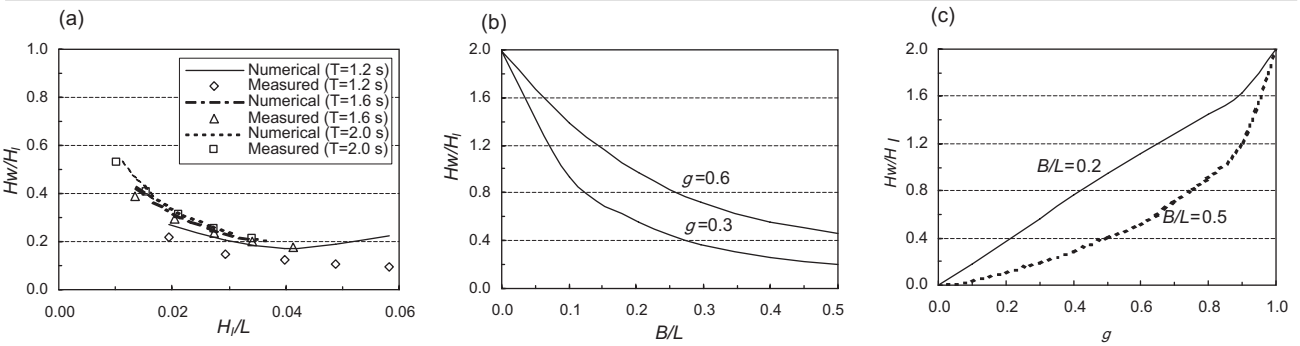

Figure 3. Non-diemensional wave height at the rear wall with (a) different incident wave conditions (b) structure width and (c) structure porosity. The results are shown for 3 wave periods and 5 wave heights in (a), while a typical wave condition T=1.6 s and H_I=0.076 m is considered in (b) and (c).

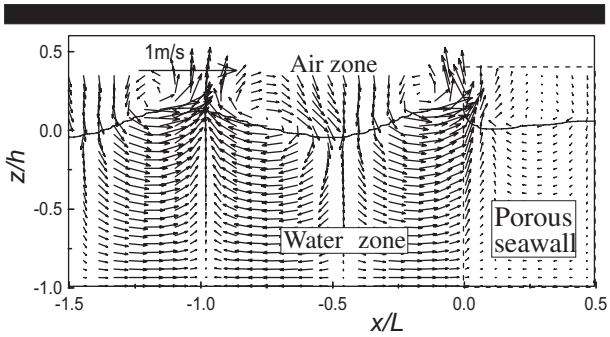

Figure 4. Velocity distributions inside and in front of the structure for a typical wave condition T=1.6 s and H_i=0.076 m.

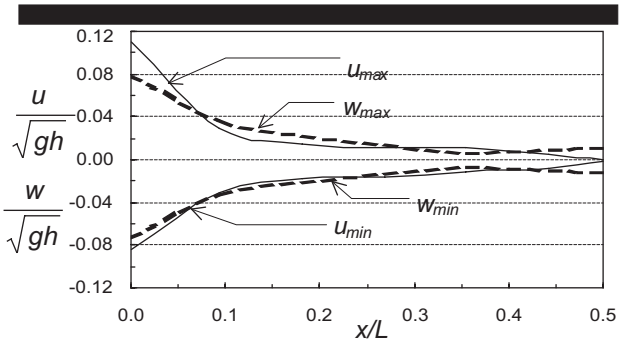

Figure 5. The maximum velocity components through the strcuture at still water level.

shown in Figure 3b. The H_w/H_i reduces exponentially with the increase of structure width. The decreasing rate follows a smooth trend for all the cases. This phenomenon can be explained in terms of velocity field and drag force. The drag force is proportional to the square of velocity. As the wave propagates inside the structure, velocity reduces with distance due to resistance forces. Consequently, wave energy, as well as wave height decreases with distance along the structure.

The effect of porosity on wave height at the rear wall is shown in Figure 3c in non-dimensional form. It can be seen that for small porosity, wave height at the rear wall is very small. In the case of small porosity, wave is mostly reflected by the front wall and structure itself. It causes less wave transmission through the structure. Consequently, wave height at the rear wall is very small. The variations of H_w/H_i are shown for B/L=0.2 and B/L=0.5. The increasing trends of H_w/H_i are not same for different structure widths. In the example of Figure 3b, wave height increases almost linearly for B/L=0.2 but it increases exponentially for B/L=0.5.

Velocity Distributions

The result of velocity field with water surface inside and in front of structure is shown in Figure 4. The thick line represents interface of water and air zone. The results are shown for the height of 1.33 h from the bottom (the same height of porous structure), which includes small part of air zone. In the figure, the velocity vectors are shown at every 8th grid in x direction and every 2nd grid in z direction. It can be seen that velocities just inside and just outside the structure are almost same in magnitude but different in phases. Partial standing wave motion is observed in front of the structure. The phase difference is also considerable as the wave run-up and run-down are delayed inside the structure. The velocity decreases sharply towards the rear wall.

The variations of velocity components through the structure are investigated for the same wave and structural conditions as above. In Figure 5, computed maximum and minimum velocities at the still water level are shown for horizontal velocity u and vertical velocity w. Both components decrease sharply along the structure. At the beginning, decreasing rate for horizontal velocity is very large while vertical velocity decreases monotonously. It shows that horizontal velocity decreases greatly within very short distance inside the structure and reaches to almost constant velocity close to x/L=0.2. The vertical velocity, however, decreases gradually. The effective structure width for wave energy dissipation can be explained in terms of spatial velocity distributions. The influential term for energy dissipation is the drag force which is proportional to quadric of velocity. As to our observation, velocity is nearly constant after some distance inside the structure. It implies that energy dissipation nearly constant after certain relative structure width.

CONCLUSION

A numerical model is developed to simulate the wave motion in and around the porous structure based on adapted Navier-Stokes equations with proper calibration and verification. The model is applied to investigate the influences of structure width and porosity on reflection and wave height at the rear wall. The reflection is influenced considerably by the structure width in the range of B/L0.2. It is almost constant for B/L0.4. Based on the numerical investigations, positive role of porosity in reducing wave reflection is confirmed. The reflection is very small in the region of 0.60.8. The influences of structure width and porosity on wave height at the rear wall, however, are different from the reflection. It is observed that wave height at the rear wall decreases exponentially with increasing structure width and increases with porosity increasing monotonously.

The result in this study gives an overall idea of velocity distributions around the porous structure. It is confirmed that partial standing wave motion is formed in front of the structure. The velocity distributions at the front face are similar both inside and outside of the structure, which confirms the continuity of flow. The phase difference is also considerable as the wave run-up and run-down are delayed inside the structure. The velocity decreases along the structure significantly and near the rear wall it approaches zero. This is due to the strong energy dissipation along the structure. As a result, wave force on the rear wall is very small. The porous layer acts as a buffer, absorbing the wave energy and attenuates the flow impact on the rear wall. This implies that porous layer is very effective for the protection of any coastal structures.

LITERATURE CITED

HARVIE, D.J.E. and FLETCHER, D.F., 2001. A new volume of fluid advection algorithm: The defined donating region scheme, *J. of Numerical Methods in Fluids*, 35, 151-172.

HIEU, P.D. and TANIMOTO, K., 2002. A two-phase flow model for simulation of wave transformation in shallow water, *Proceedings of the 4th International Summer Symposium* (Kyoto, Japan, JSCE), pp.179-182.

HIRT, C.W. and NICHOLS, B.D., 1981. Volume of fluid (VOF) method for the dynamics of free boundaries, *Journal of Computational Physics*, 39, 201-225.

KARIM, M.F.; TANIMOTO, K. and HIEU, P.D., 2003. Simulation of wave transformation in vertical permeable structure, *Proc. 13th International Offshore and Polar Engg. Conference* (Hawaii, USA, ISOPE), pp.727-733.

MALLAYACHARI, V. and SUNDAR, V., 1994. Reflection characteristics of permeable seawalls, *Coastal Engineering*, 23, 135-150.

SAKAKIYAMA, T. and KAJIMA, R., 1992. Numerical simulation of nonlinear wave interacting with permeable breakwaters, *Proc. 23rd Int. Conference on Coastal Engineering* (Venice, Italy, ASCE), pp.1517-1530.

SUSSMAN, M.; SMEREKA, P. and OSHER, S., 1994. A level set approach for computing solutions to incompressible two-phase flow, *Journal of Computational Physics*, 114, 146-159. van GENT, M.R.A., 1995. Porous flow through rubble mound material, Journal of Waterways, Port, Coastal and Ocean Engineering, 121 (3), 176-181.